*Archives of Hydro-Engineering and Environmental Mechanics*
Vol. 52 (2005), No. 1, pp. 39–58
© IBW PAN, ISSN 1231–3726

# Loads Exerted by Floating Ice on a Cylindrical Structure

**Ryszard Staroszczyk**

Institute of Hydro-Engineering, Polish Academy of Sciences
ul. Waryńskiego 17, 71-310 Szczecin, Poland, e-mail: r.star@ibwpan.szczecin.pl

(Received December 23, 2004; revised February 14, 2005)

## Abstract

The paper is concerned with the problem of interaction between a coherent floating ice cover and a fixed, rigid, vertically-walled circular cylinder. The ice cover, of horizontal dimensions considerably larger than the size of the structure, is assumed to be driven against the structure by wind and water current drag stresses. The floating ice cover is modelled as a plate that is subject to the action of horizontal forces and transverse bending due to the reaction of underlying water. During an interaction event, of a quasi-static character, the ice is modelled as a creeping material the behaviour of which is described by a viscous flow law with two, bulk and shear, viscosities. The viscosities change dramatically in their magnitudes during a transition from converging to diverging deformation of the material to reflect the fact that floating ice offers much less resistance to tensile rather than compressive stresses. By numerical simulations carried out by a finite difference method, the influence of the ice rheological parameters on the distribution of contact stresses at the ice – structure interface is investigated. Two types of boundary conditions at the interface, free-slip and no-slip, are considered, and their effects on the loads sustained by the structure are compared. In addition, creep buckling of the ice sheet near the structure is analysed to determine the critical time at which ice starts to fail due to exceeding its flexural strength at given loading conditions.

**Key words**: floating ice, plate, rheology, creep buckling, finite difference method

## Notations

| | | |
|---|---|---|
| $D_{rr}$, $D_{\theta\theta}$, $D_{r\theta}$ | – | strain-rate components, |
| $\boldsymbol{D}$ | – | strain-rate tensor, |
| $g$ | – | gravitational acceleration, |
| $h$ | – | ice plate thickness, |
| $\boldsymbol{I}$ | – | unit tensor, |
| $J_1$, $J_2$ | – | parameters defining in-plane creep behaviour of a plate, |
| $K$, $K_1$, $K_2$ | – | parameters defining flexural creep behaviour of a plate, |
| $M_r$, $M_\theta$ | – | bending moments per unit width of a plate, |

$M_{r\theta}$ – twisting moment per unit width of a plate,
$N_r$, $N_\theta$ – axial in-plane forces per unit width of a plate,
$N_{r\theta}$ – shear in-plane force per unit width of a plate,
$Q_r$, $Q_\theta$ – transverse shear forces per unit width of a plate,
$q_r, q_\theta, q_z$ – distributed load intensities,
$p$ – mean pressure in ice,
$r, \theta, z$ – cylindrical polar coordinates,
$R_0$ – cylinder radius,
$v_r$, $v_\theta$ – horizontal ice velocity components,
$w$ – plate deflection,
$z_0$ – plate neutral plane position,
$\gamma, \eta$ – strain-rate invariants,
$\zeta, \zeta_a$ – bulk and axial viscosities of ice,
$\kappa_r$, $\kappa_\theta$ – curvatures of a plate deflection surface,
$\kappa_{r\theta}$ – twist of a plate deflection surface,
$\mu$ – shear viscosity of ice,
$\sigma_{rr}, \sigma_{\theta\theta}, \sigma_{r\theta}$ – stress components,
$\boldsymbol{\sigma}, \hat{\boldsymbol{\sigma}}$ – stress tensor, deviatoric stress tensor.

## 1. Introduction

The problem of determination of forces to which an off-shore structure is subject during its interaction with a floating ice cover is of great importance in engineering practice, and has therefore been studied in the past thirty years for a range of structures of various shapes and dimensions, and in different ice conditions. Nevertheless, despite all the effort, often ambiguous and still inconclusive, results are obtained due to the difficulties associated with the proper description of the rheology of sea ice. Depending on the strain, strain-rate, and stress levels in ice, the material behaviour varies from purely elastic in dynamic events (such as an ice floe impact on a structure), to viscoelastic in events taking place for several minutes (interaction between moving vessels and the ice), to plastic, viscoplastic, or viscous behaviour in events lasting for hours and days when the creep behaviour of ice becomes a dominant form of the material deformation. The latter is the type of problem we are concerned with in this paper. More specifically, our focus is on the problem in which an engineering structure of a circular shape interacts with an ice field of characteristic dimensions significantly larger than the size of the object, during a quasi-static event in which the ice is driven onto the structure due to the action of wind.

We assume that the floating ice sheet is coherent enough to be treated as a continuous cover in the horizontal plane, as opposed to a multitude of individual,

loosely connected floes that interact with one another in a series of separate events. We also suppose that, due to the typical stress levels (less than 1 MPa) occurring in the problem, and the slowness of the processes taking place, the behaviour of ice is ductile, i.e., no brittle failure mechanisms are considered. A further simplification is that the ice is flat enough to be treated as a plate of an approximately uniform thickness, spreading on the water surface. A similar problem to that analysed here, of a circular cylinder interacting with a creeping plate of ice, has previously been investigated by Wang, Ralston (1983) and Sjölind (1985). In the first of these papers, the ice is treated as an elastic-plastic material, while in the other, a viscoelastic rheology has been adopted to describe the ice deformation. In our study the creep behaviour of ice is modelled by a non-linearly viscous flow law in which the material viscosities depend very strongly on the current dilatation rate. Such an approach is motivated by the observation that the strength of ice under compression (that is, in converging flow) is by several orders of magnitude greater than under extension – in the latter case the crack-like features that develop in ice due to its divergence, prohibit the material from supporting tensile stresses.

The problem is analysed by applying the standard theory of thin plates resting on a liquid base and sustaining, beside bending, also in-plane axial and shear loading. Using the plate equilibrium equations and the viscous flow law for ice, the creep behaviour of the ice cover is described by a set of differential equations that are subsequently solved by a finite difference technique. The results of numerical simulations carried out for a range of ice rheological parameters and two different types of boundary conditions (no-slip and free-slip) at the cylinder wall, show the distribution of the contact forces at the structure – ice interface, and the variation of the ice stresses in the vicinity of the object. The influence of the ice rheology on the total horizontal force exerted by the moving ice on the cylinder is also illustrated. The numerical analysis is complemented by investigating the evolution of the plate deflection near the cylinder wall in order to show the development of creep buckles in the ice cover up to the time of its failure due to exceeding the material bearing capacity.

To a certain extent, this work is a sequel to the paper by Staroszczyk (2003) in which the interaction between a rectangular structure and an ice field is analysed. However, apart from the different shape of the structure, a different, and more complex, non-linear rheology of ice is also adopted now, compared with the linearly viscous flow law applied in the previous investigation.

## 2. Governing Equations

The floating ice cover is treated as a plate that rests on a liquid base, and is subject to the combined action of in-plane and transverse loads. The in-plane loads, acting tangentially to the plate surfaces, are caused by the wind and water

current drag forces, and the transverse load is due to the vertical reaction of the underlying water. Thus, the plate undergoes both axial and shear deformations in the horizontal plane, and bending and twisting that deforms the plate off its middle surface. Since we are concerned here with the problem involving a single circular structure, we adopt cylindrical polar coordinates $r, \theta, z$ $(0 \leq \theta < 2\pi)$, with the vertical $z$-axis coinciding with the axis of symmetry of the cylinder, as shown in Fig. 1. For simplicity, the region of the ice cover which immediately interacts with the structure is assumed to be of a constant thickness, denoted by $h$. The ice is treated as homogeneous across its depth; i.e., temperature and ice porosity variations with depth are neglected in the analysis. The $z$-axis, directed downwards, is chosen in such a way that $z = 0$ corresponds to the top surface of the plate, and $z = h$ to the bottom. The plate deflection along the $z$-axis is denoted by $w$. A circular cylinder, with a radius $R_0$, is treated as a fixed rigid body that interacts with the ice sheet along its vertical walls at $r = R_0$. Our purpose is to evaluate the horizontal forces which the floating ice exerts on the structure during an interaction event.

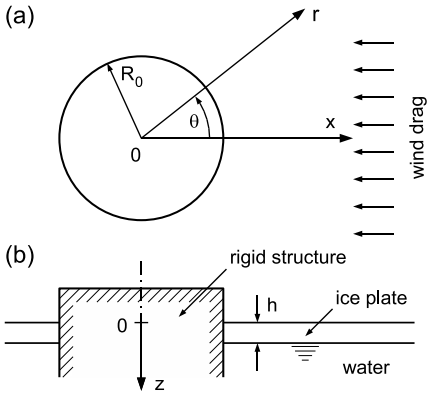


**Fig. 1.** Geometry of the problem and the adopted polar coordinates: (a) plane view, (b) plate cross-section

The problem is solved by employing the classical, linear theory of thin plates (Timoshenko and Woinowsky-Krieger 1959) based on the assumptions that the plate thickness $h$ is small as compared with its span, the plate transverse displacements $w$ are, at most, of the order of the plate thickness, and the plate cross-sections which were normal to the middle plane in the undeformed state remain so during the deformation.

The definitions of internal forces acting on an infinitesimal plate element, with components expressed in the adopted polar coordinates, are given in Fig. 2. The axial forces acting in the horizontal plane $Or\theta$ are denoted by $N_r$ and $N_\theta$, and the in-plane shear forces are $N_{r\theta} = N_{\theta r}$, all measured per unit length along the

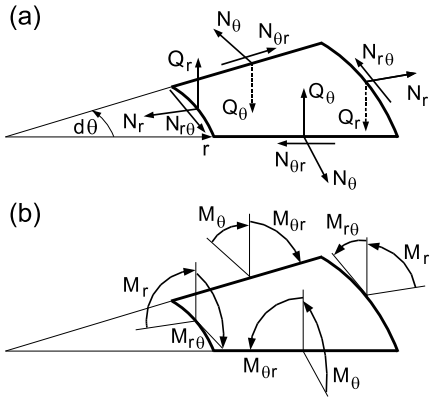


**Fig. 2.** Definitions of internal forces acting on a plate element: (a) axial and shear forces, (b) bending and twisting moments.

plate span. The external forces acting in the horizontal direction are those coming from the wind and water drag; their components are denoted by $q_r$ and $q_\theta$. Then, in the absence of inertia forces neglected here due to small variations in the ice velocities, the equilibrium equations are expressed by

$$\begin{aligned} &\frac{\partial(rN_r)}{\partial r} - N_\theta + \frac{\partial N_{\theta r}}{\partial \theta} + rq_r = 0, \\ &\frac{1}{r}\frac{\partial(r^2 N_{r\theta})}{\partial r} + \frac{\partial N_\theta}{\partial \theta} + rq_\theta = 0. \end{aligned} \tag{1}$$

Along the $z$-direction, a plate element is subject to vertical shear forces $Q_r$ and $Q_\theta$, and also to the transverse distributed load $q_z$ coming from the underlying water. Since in our problem, the in-plane forces $N_r$, $N_\theta$ and $N_{r\theta}$, all acting in the directions tangential to the deflection surface $w(r, \theta)$, can be of magnitudes considerably greater than those of the vertical shear forces $Q_r$ and $Q_\theta$, we include the $z$-components of the former in the equilibrium balance. Accordingly, neglecting the own weight of ice, the projection of all forces in the vertical direction gives

$$\begin{aligned} &\frac{\partial(rQ_r)}{\partial r} + \frac{\partial Q_\theta}{\partial \theta} + \frac{\partial}{\partial r}\left(rN_r\frac{\partial w}{\partial r}\right) + \frac{1}{r}\frac{\partial}{\partial \theta}\left(N_\theta\frac{\partial w}{\partial \theta}\right) \\ &\quad + \frac{\partial}{\partial r}\left(N_{r\theta}\frac{\partial w}{\partial \theta}\right) + \frac{\partial}{\partial \theta}\left(N_{\theta r}\frac{\partial w}{\partial r}\right) + rq_z = 0, \end{aligned} \tag{2}$$

involving, apart from the internal forces, also plate deflection derivatives. Equilibrium of all moments (see Fig. 2b) acting on an infinitesimal plate element with

respect to the radial and circumferential directions yields the expressions

$$\begin{aligned} \frac{\partial (r M_r)}{\partial r} - \frac{\partial M_{\theta r}}{\partial \theta} - r Q_r = 0, \\ \frac{\partial M_\theta}{\partial \theta} - \frac{\partial (r M_{r\theta})}{\partial r} - r Q_\theta = 0, \end{aligned} \tag{3}$$

where $M_r$ and $M_\theta$ are the bending moments, and $M_{r\theta} = M_{\theta r}$ the twisting moments, all per unit length. Elimination of the shear forces $Q_r$ and $Q_\theta$ from (2) by means of the relations (3) gives

$$\begin{aligned} \frac{\partial^2 (r M_r)}{\partial r^2} + \frac{1}{r}\frac{\partial^2 M_\theta}{\partial \theta^2} - \frac{\partial^2 M_{r\theta}}{\partial r \partial \theta} - \frac{1}{r}\frac{\partial^2 (r M_{r\theta})}{\partial r \partial \theta} + r N_r \frac{\partial^2 w}{\partial r^2} + N_\theta \left( \frac{1}{r}\frac{\partial^2 w}{\partial \theta^2} + \frac{\partial w}{\partial r} \right) \\ + 2 r N_{r\theta} \frac{\partial^2}{\partial r \partial \theta}\left(\frac{w}{r}\right) - r q_r \frac{\partial w}{\partial r} - q_\theta \frac{\partial w}{\partial \theta} + r q_z = 0. \end{aligned} \tag{4}$$

The external forces that drive the system are represented by the distributed loads $q_r$, $q_\theta$, and $q_z$. The latter transverse load is the result of the response of the underlying liquid, and is assumed to be proportional to the plate deflection. Hence,

$$q_z = -\varrho_w g w, \tag{5}$$

where $\varrho_w$ denotes the water density, and $g$ is the acceleration due to gravity. The tangential forces with component intensities $q_r$ and $q_\theta$ express the effect of wind and water action. Quadratic relations are adopted for the wind and water drag tractions, expressed by

$$\boldsymbol{\tau}_a = C_a \varrho_a (\boldsymbol{u}_a - \boldsymbol{v}) |\boldsymbol{u}_a - \boldsymbol{v}|, \qquad \boldsymbol{\tau}_w = C_w \varrho_w (\boldsymbol{u}_w - \boldsymbol{v}) |\boldsymbol{u}_w - \boldsymbol{v}|, \tag{6}$$

where $\boldsymbol{\tau}_a$ and $\boldsymbol{\tau}_w$ are the tangential tractions due to wind stress and water drag, respectively, dimensionless parameters $C_a$ and $C_w$ are the wind and water drag coefficients (Sanderson 1988), $\varrho_a$ denotes the air density, $\boldsymbol{u}_a$ and $\boldsymbol{u}_w$ are the velocity vectors of wind and water current, and $\boldsymbol{v}$ is the horizontal velocity of ice. Loads $q_r$ and $q_\theta$ are the sums of the projections of $\boldsymbol{\tau}_a$ and $\boldsymbol{\tau}_w$ on the respective directions $r$ and $\theta$.

The internal forces in the plate are given by the depth integration of the axial, $\sigma_{rr}$ and $\sigma_{\theta\theta}$, and shear, $\sigma_{r\theta}$, stresses. Therefore, the in-plane forces are defined by

$$N_r = \int_0^h \sigma_{rr} \mathrm{d}z, \quad N_\theta = \int_0^h \sigma_{\theta\theta} \mathrm{d}z, \quad N_{r\theta} = \int_0^h \sigma_{r\theta} \mathrm{d}z, \tag{7}$$

and the bending and twisting moments by

$$M_r = \int_0^h \sigma_{rr} z \mathrm{d}z, \quad M_\theta = \int_0^h \sigma_{\theta\theta} z \mathrm{d}z, \quad M_{r\theta} = -\int_0^h \sigma_{r\theta} z \mathrm{d}z. \tag{8}$$

The stresses required in (7) and (8) are related to ice deformations through constitutive equations. In the problem considered in this study we are concerned with the material behaviour in which creep, i.e., irreversible deformations, dominate reversible strains due to elastic and viscoelastic response of ice. Therefore, we describe the material deformation by means of strain-rates. Here, we assume the creep properties of ice in compression to be substantially different from those in extension. Hence, in general, the neutral plane in the ice plate subject to bending does not coincide with its middle plane, and this should be taken into account in a rigourous treatment of the problem. We note however, that in typical engineering problems of interest (young, that is, flat and undistorted ice, and relatively short time scales involved), the stresses due to in-plane deformation of ice are much greater in magnitude than those due to bending – only at instants prior to the onset of the ice flexural failure do the latter become a major factor. For this reason, we simplify the analysis by neglecting the effects of bending on the mean creep properties of ice across its thickness, and subsequently assume the neutral plane of the ice plate to coincide with its middle plane.

The axial and shear behaviour of the ice plate which occurs in its middle plane, is determined by the horizontal velocity field. Denoting the components of the horizontal velocity vector $\boldsymbol{v}$ by $v_r$ and $v_\theta$, the components of the associated in-plane strain-rate tensor $\boldsymbol{D}$ are expressed by

$$D_{rr} = \frac{\partial v_r}{\partial r}, \quad D_{\theta\theta} = \frac{1}{r}\left(v_r + \frac{\partial v_\theta}{\partial \theta}\right), \quad D_{r\theta} = \frac{1}{2}\left[\frac{1}{r}\frac{\partial v_r}{\partial \theta} + r\frac{\partial}{\partial r}\left(\frac{v_\theta}{r}\right)\right]. \tag{9}$$

Strain-rates occurring due to bending and twisting of the plate are, in turn, determined by the time rates of the curvatures and twist of the deflection surface $w$. Hence,

$$D_{rr} = \dot{\kappa}_r z', \quad D_{\theta\theta} = \dot{\kappa}_\theta z', \quad D_{r\theta} = -\dot{\kappa}_{r\theta} z', \quad z' = z - z_0, \tag{10}$$

where $\kappa_r$ and $\kappa_\theta$ denote the curvatures along the $r$ and $\theta$ coordinates, respectively, $\kappa_{r\theta}$ denotes the plate twist, and $z' = z - z_0$ is the distance from the neutral plane, with $z_0$ defining the position of the latter in the undeformed state. In terms of the plate deflection $w(r, \theta)$, the curvatures and the twist are given by

$$\kappa_r = -\frac{\partial^2 w}{\partial r^2}, \quad \kappa_\theta = -\frac{1}{r}\frac{\partial w}{\partial r} - \frac{1}{r^2}\frac{\partial^2 w}{\partial \theta^2}, \quad \kappa_{r\theta} = \frac{\partial}{\partial r}\left(\frac{1}{r}\frac{\partial w}{\partial \theta}\right). \tag{11}$$

Specific forms of the stress – strain-rate relations depend on a type of rheology that is adopted to describe the creep of floating ice. These are discussed in the following Section.

## 3. Creep Behaviour of Floating Ice

Commonly, the creep behaviour of floating ice is described by either the viscoplastic or viscous constitutive relations. The more complex viscoplastic theories

are based on the formulation by Hibler (1979), with a later modification by Hibler and Ip (1995), which describe distinct responses above and below a critical value of a strain-rate invariant (a combination of the dilatation rate and shear rate invariant). Above the critical strain-rate level, the stresses in ice lie on a yield curve, while below the critical level the stresses are determined by a viscous flow relation. A simpler approach is based on the Reiner-Rivlin viscous fluid constitutive law, originally proposed for sea ice applications by Smith (1983), and then followed by Overland and Pease (1988) and others. The comparisons between the predictions of these two classes of laws are made by Schulkes, Morland and Staroszczyk (1998), who have applied four different ice rheologies to the simulations of ice pack behaviour on a geophysical scale. A form of the constitutive law that combines the features of the viscoplastic and viscous rheologies has been proposed by Gray and Morland (1994) and Morland and Staroszczyk (1998), in which the response of ice is viscous for any (positive) dilatation rate, but is bounded by a stress envelope for higher values of the deformation rates.

We confine our attention here to a Reiner-Rivlin constitutive relation. A general, frame-indifferent, two-dimensional equation for a viscous material, which expresses the Cauchy stress $\boldsymbol{\sigma}$ in terms of the strain-rate $\boldsymbol{D}$, has the form

$$\boldsymbol{\sigma} = \phi_1(S_i, \eta, \gamma)\,\boldsymbol{I} + \phi_2(S_i, \eta, \gamma)\;\boldsymbol{D}, \tag{12}$$

where $\boldsymbol{I}$ is the unit tensor, $S_i$ are scalars representing any number of state variables, and $\eta$ and $\gamma$ are two invariants of the strain-rate tensor given by

$$\eta = \operatorname{tr}\boldsymbol{D}, \quad \gamma^2 = \frac{1}{2}\operatorname{tr}\hat{\boldsymbol{D}}^2. \tag{13}$$

$\hat{\boldsymbol{D}}$ is the strain-rate deviator defined by

$$\hat{\boldsymbol{D}} = \boldsymbol{D} - \frac{1}{2}\eta\boldsymbol{I}. \tag{14}$$

In terms of the strain-rate components (9), the two invariants, the dilatation-rate $\eta$ and the shear-rate invariant $\gamma$, are expressed by

$$\eta = D_{rr} + D_{\theta\theta} = \frac{\partial v_r}{\partial r} + \frac{1}{r}\left(v_r + \frac{\partial v_\theta}{\partial \theta}\right), \quad \gamma^2 = D_{r\theta}^2 + \frac{1}{4}\left(D_{rr} - D_{\theta\theta}\right)^2. \tag{15}$$

Define also a deviatoric stress $\hat{\boldsymbol{\sigma}}$

$$\hat{\boldsymbol{\sigma}} = \boldsymbol{\sigma} + p\boldsymbol{I}, \quad p = -\frac{1}{2}\operatorname{tr}\boldsymbol{\sigma}, \tag{16}$$

where $p$ is a mean pressure in ice. The general flow law (12) can be expressed in a more conventional form, by defining the material response in terms of viscosities. To this aim, we specify the separate bulk and shear responses by taking,

respectively, the trace and the deviatoric parts of both sides of (12), which yields

$$-p = \frac{1}{2}\mathrm{tr}\boldsymbol{\sigma} = \phi_1 + \frac{1}{2}\phi_2\eta, \quad \hat{\boldsymbol{\sigma}} = \phi_2 \boldsymbol{D}. \tag{17}$$

Introducing the standard bulk viscosity $\zeta$ and the shear viscosity $\mu$ defined by

$$-p = \zeta\eta, \quad \hat{\boldsymbol{\sigma}} = 2\mu \boldsymbol{D}, \tag{18}$$

the response functions $\phi_1$ and $\phi_2$ are expressed by

$$\phi_1 = (\zeta - \mu)\eta, \quad \phi_2 = 2\mu, \tag{19}$$

by which the constitutive law (12) becomes

$$\boldsymbol{\sigma} = (\zeta - \mu)\eta\boldsymbol{I} + 2\mu \boldsymbol{D}. \tag{20}$$

In the simplest, linearly viscous, case of the flow law (20), the viscosities $\zeta$ and $\mu$ are constants. We focus here on a non-linear case in which the viscosities depend on a sole strain-rate invariant, the dilatation rate $\eta = \mathrm{tr}\,\boldsymbol{D}$, in order to account, in the constitutive equation for the fact that the strength of floating ice decreases very rapidly during a change from converging ($\eta < 0$) to diverging flow ($\eta > 0$). Gray and Morland (1994) and Schulkes, Morland and Staroszczyk (1998) investigated a class of constitutive laws with an abrupt cut-off to zero stress in diverging flow, by multiplying both viscosities by the Heaviside unit function $H(-\eta)$. Such forms, when applied to one-dimensional flows, enabled the analysis of moving interfaces separating converging and diverging regions in floating ice packs under varying wind conditions (Gray and Morland 1994). However, attempts to use the flow laws with the Heaviside function in two-dimensional flows failed, since numerical instabilities arose in the numerical solution (Schulkes, Morland and Staroszczyk 1998). Therefore, to remedy the situation, Morland and Staroszczyk (1998) replaced the abrupt cut-off by a smooth transition to zero stress over a dilatation rate range equal to approximately one-tenth to one-hundredth of the maximum convergence rate in the problem, which led to a stable algorithm in the analysis of ice pack behaviour on the geophysical scale. Shifting the smooth transition into the converging regime, to avoid any tensile stress, proved not as effective. In our, engineering scale problem considered here, we pursue a similar approach, in which both viscosities are reduced in a smooth manner over a narrow range of divergence rates $\eta$ close to zero. Thus, we adopt a scaling factor $\bar{H}(\eta)$ defined by

$$\bar{H}(\eta) = \begin{cases} 1 & \text{if} \quad \eta < 0, \\ \exp\left[-(\eta/\eta_c)^2\right] & \text{if} \quad \eta \geq 0, \end{cases} \tag{21}$$

which is unity at $\eta = 0$, tends to zero as $\eta \to \infty$, and has zero derivatives at $\eta = 0$. The free parameter $\eta_c$ is a divergence rate magnitude around which significant

changes in viscosities occur. Accordingly, with the function $\bar{H}$, the flow law (20) is modified to take the form

$$\boldsymbol{\sigma} = [(\zeta - \mu)\eta \boldsymbol{I} + 2\mu\, \boldsymbol{D}]\, \bar{H}(\eta). \tag{22}$$

The above constitutive relation is now employed to express the internal forces in the ice sheet in terms of horizontal velocities and plate deflection. Hence, the stress components determined by (22), when inserted into the definitions (7) along with the strain-rates given by (9), yield the in-plane axial and shear forces

$$\begin{aligned} N_r &= (J_1 + J_2)\frac{\partial v_r}{\partial r} + (J_1 - J_2)\,\frac{1}{r}\left(v_r + \frac{\partial v_\theta}{\partial \theta}\right), \\ N_\theta &= (J_1 - J_2)\frac{\partial v_r}{\partial r} + (J_1 + J_2)\,\frac{1}{r}\left(v_r + \frac{\partial v_\theta}{\partial \theta}\right), \\ N_{r\theta} &= J_2\left[\frac{\partial v_\theta}{\partial r} + \frac{1}{r}\left(\frac{\partial v_r}{\partial \theta} - v_\theta\right)\right]. \end{aligned} \tag{23}$$

Similarly, the definitions (8), when combined with a relations (22), (10) and (11), determine the bending and twisting moments as

$$\begin{aligned} M_r &= -\left[(K_1 + K_2)\,\frac{\partial^2 \dot{w}}{\partial r^2} + (K_1 - K_2)\,\frac{1}{r}\left(\frac{\partial \dot{w}}{\partial r} + \frac{1}{r}\frac{\partial^2 \dot{w}}{\partial \theta^2}\right)\right], \\ M_\theta &= -\left[(K_1 - K_2)\,\frac{\partial^2 \dot{w}}{\partial r^2} + (K_1 + K_2)\,\frac{1}{r}\left(\frac{\partial \dot{w}}{\partial r} + \frac{1}{r}\frac{\partial^2 \dot{w}}{\partial \theta^2}\right)\right], \\ M_{r\theta} &= 2K_2\,\frac{\partial^2}{\partial r\,\partial \theta}\left(\frac{\dot{w}}{r}\right). \end{aligned} \tag{24}$$

In expressions (23) and (24), the parameters defining the viscous properties of the ice sheet are given by

$$J_1 = \int_0^h \bar{\xi}\,\mathrm{d}z, \quad J_2 = \int_0^h \bar{\mu}\,\mathrm{d}z, \quad K_1 = \int_0^h \bar{\xi} z(z - z_0)\mathrm{d}z, \quad K_2 = \int_0^h \bar{\mu} z(z - z_0)\mathrm{d}z, \tag{25}$$

where

$$\bar{\xi} = \zeta \bar{H}(\eta), \quad \bar{\mu} = \mu \bar{H}(\eta). \tag{26}$$

Substitution of the moment expressions (24) into the equilibrium relation (4), with $q_z$ given by (5), yields the differential equation for the plate deflection function $w$ in the form

$$\begin{aligned} K\nabla^2\nabla^2 \dot{w} = N_r\,\frac{\partial^2 w}{\partial r^2} + N_\theta \frac{1}{r}\left(\frac{\partial w}{\partial r} + \frac{1}{r}\frac{\partial^2 w}{\partial \theta^2}\right) + 2N_{\theta r}\,\frac{\partial^2}{\partial r\,\partial \theta}\left(\frac{w}{r}\right) \\ - q_r\,\frac{\partial w}{\partial r} - \frac{q_\theta}{r}\,\frac{\partial w}{\partial \theta} - \varrho_w g\, w, \end{aligned} \tag{27}$$

where

$$\nabla^2 = \frac{\partial^2}{\partial r^2} + \frac{1}{r}\frac{\partial}{\partial r} + \frac{1}{r^2}\frac{\partial^2}{\partial \theta^2} \tag{28}$$

is the Laplace operator, and

$$K = K_1 + K_2 = \int_0^h \bar{\zeta}_a z(z - z_0)\mathrm{d}z \tag{29}$$

is the parameter defining the flexural viscous response of the ice plate. In (29), $\bar{\zeta}_a$ is the axial viscosity which describes the response of ice to uniaxial, laterally confined, compression, and is defined by

$$\bar{\zeta}_a = \bar{\zeta} + \bar{\mu}. \tag{30}$$

The in-plane forces $N_r$, $N_\theta$ and $N_{r\theta}$, appearing in (27) and required to determine the plate deflection evolution, can be determined independently of (27) by solving the horizontal equilibrium equations (1) with the in-plane forces expressions (23).

## 4. Numerical Simulations

The system of differential equations (1) with (23) for the horizontal velocities $v_r$ and $v_\theta$ and (27) for the plate deflection $w$ has been solved approximately by a finite difference method. Due to the symmetry of the problem with respect to the direction of wind which is assumed to blow along the coordinate line $\theta = 0$, only the domain $0 \leq \theta \leq \pi$ is considered in the numerical model. In the radial direction, the ice domain extends from the cylinder wall at $r = R_0$ to the free edge of the ice cover at $r = R_{\max}$. The computational mesh has 300 nodes in the radial direction and 51 nodes in the circumferential direction (15300 nodes in all), uniformly distributed along both $\theta$ and $r$. All partial derivatives have been approximated by standard central differences.

The results of numerical simulations presented below have been carried out for the ice viscosities $\zeta = 2.0 \times 10^9$ kg m$^{-1}$s$^{-1}$ and $\mu = 1.0 \times 10^9$ kg m$^{-1}$s$^{-1}$, which can be regarded as typical viscosity magnitudes for floating ice. As the maximum horizontal strain-rates occurring in our problem are of magnitudes equal to about $5 \times 10^{-5}$ s$^{-1}$, the free material parameter $\eta_c$ that describes the ice strength reduction rate at the onset of diverging deformation has been adopted from within a range embracing the latter value. Hence, $\eta_c$ has been chosen to vary from $5 \times 10^{-6}$ to $1 \times 10^{-4}$ s$^{-1}$ to explore the influence of $\eta_c$ on the magnitudes of the contact forces at the cylinder wall, as well as the stress field in the ice cover. The dimensionless wind and drag coefficients appearing in (6) have been assumed of the values $C_a = 2 \times 10^{-3}$ and $C_w = 4 \times 10^{-3}$ (Sanderson 1988). The air and water densities are $\varrho_a = 1.3$ kgm$^{-3}$ and $\varrho_w = 1.02 \times 10^3$ kgm$^{-3}$, and

$g = 9.81$ ms$^{-2}$. At the ice – structure interface either the no-slip (full bonding) or free-slip boundary conditions are assumed for the horizontal deformation of the ice, and simply-supported conditions for the plate bending. These are expressed for a no-slip boundary by

$$r = R_0: \quad \boldsymbol{v} = 0, \quad w = 0, \quad M_r = 0, \tag{31}$$

and for a free-slip boundary by

$$r = R_0: \quad \boldsymbol{v} \cdot \boldsymbol{n} = 0, \quad N_{r\theta} = 0, \quad w = 0, \quad M_r = 0, \tag{32}$$

where $\boldsymbol{n}$ is the unit vector normal to the cylinder wall. The ice at the outer edge $r = R_{\max}$ is assumed to be stress-free, that is,

$$r = R_{\max}: \quad N_r = 0, \quad N_{r\theta} = 0. \tag{33}$$

Simulations have been conducted for a cylinder of the radius $R_0 = 10$ m, situated at the centre of a circular ice field spreading to $R_{\max} = 500$ m. The thickness of the ice cover is $h = 0.2$ m. The ice is pushed onto the structure by a wind with a velocity of $u_a = 30$ ms$^{-1}$, blowing along the coordinate line $\theta = 0$ in the negative direction of $r$. Such a wind produces a tangential stress $\tau_a$ on the ice surface with a magnitude of about 2.3 Pa. It is assumed that there are no water currents in the area of interest that could generate additional drag forces on the ice. The plots in Figures 3 and 4 show the distribution of the forces exerted by the ice on the cylinder wall in the case of a no-slip boundary. Illustrated is the dependence of the loads on the value of the rheological parameter $\eta_c$. For comparison, the contact forces generated in the case of a linearly viscous response of ice are also depicted. Figure 3 shows the variation of the radial force $N_r$ with the angle $\theta$. We note that the effect of the ice viscosity reduction in diverging flow occurring on the leeward side of the cylinder ($\theta > 90^\circ$) is hardly observed on the part of the wall subject to the compressive stresses from the ice ($\theta < 90^\circ$). In fact, the radial forces $N_r$ (in our geometry normal to the wall) on the windward side of the cylinder are practically insensitive to $\eta_c$, and are approximately the same as for the linearly viscous ice. In contrast, on the leeward side of the cylinder a dramatic decrease in the magnitude of $N_r$ is observed for values of $\eta_c$ smaller than the typical dilatation rate $\eta$ near the structure; in our case the latter is about $5 \times 10^{-5}$ s$^{-1}$.

A similar pattern is seen in Figure 4 illustrating the variation of the shear forces $N_{r\theta}$ with the angle $\theta$ and rheological parameter $\eta_c$. Again, the tangential forces exerted on the windward side of the cylinder are roughly independent of $\eta_c$, while on the leeward side the contact forces on the wall rapidly approach zero with $\eta_c < 5 \times 10^{-5}$ s$^{-1}$ decreasing. Comparing this figure with the previous one, the change in the loading coming from the ice cover, for small values of $\eta_c$, seems even more dramatic.

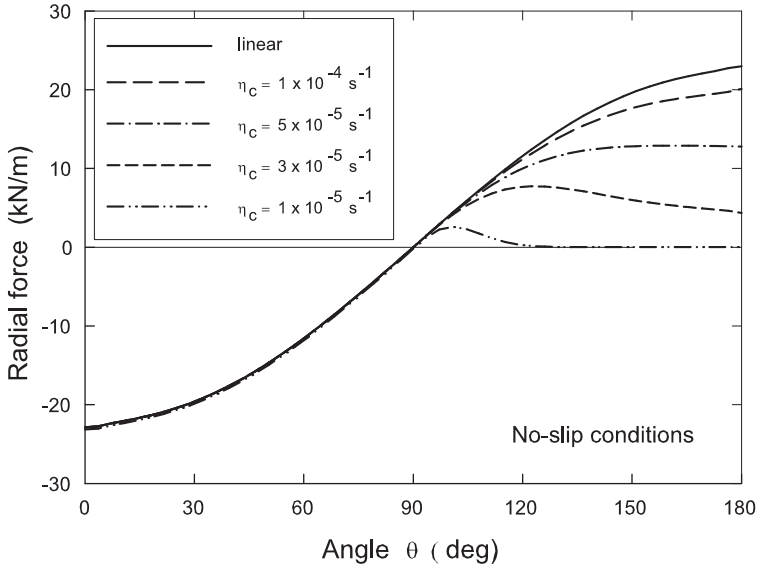


**Fig. 3.** Distribution of the radial forces $N_r$ along the cylinder wall for no-slip boundary conditions and different magnitudes of the rheological parameter $\eta_c$

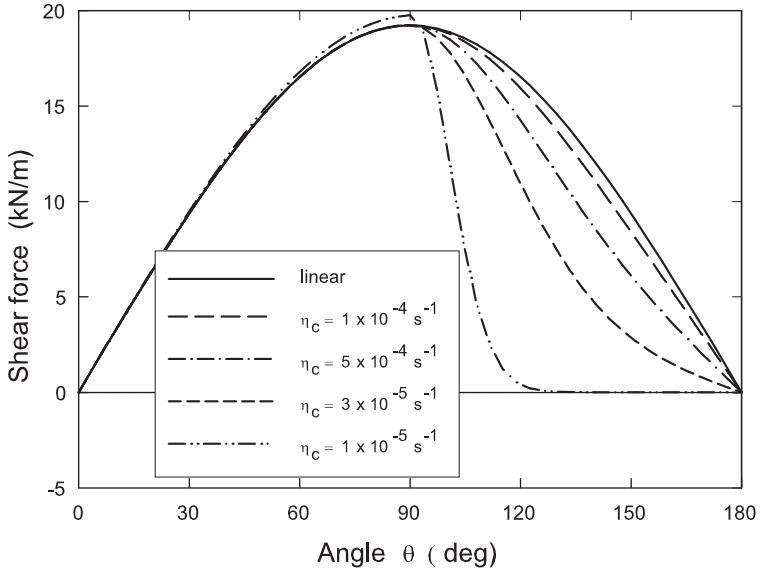


**Fig. 4.** Distribution of the shear forces $N_{r\theta}$ along the cylinder wall for no-slip boundary conditions and different magnitudes of the rheological parameter $\eta_c$

Figure 5 displays the distribution of the normal forces $N_r$ on the cylinder wall in the case of a free-slip boundary, when the tangential forces $N_{r\theta}$ are zero. As now the floating ice does not exert any shear stresses on the structure, more load is passed on the cylinder through the normal contact forces. Hence, the maximum normal reactions, at $\theta = 0$, are about 40 per cent greater than in the case of no-slip at the interface, see Fig. 3. Otherwise, qualitatively very similar features are observed as in the case of no-slip between the ice and the structure, with practically unchanged contact loading on the windward wall and a significant reduction of the $N_r$ forces on the leeward side for dilatation rates $\eta_c < 5 \times 10^{-5}$ s$^{-1}$.

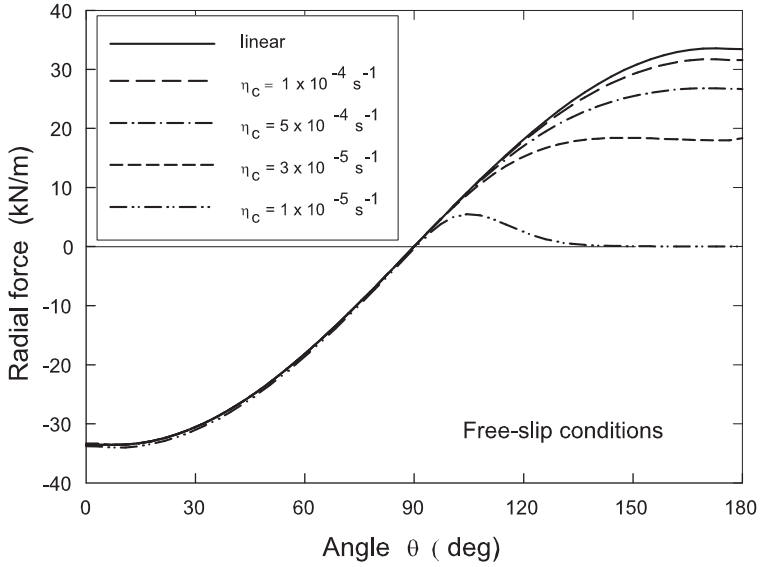


**Fig. 5.** Distribution of radial forces $N_r$ along the cylinder wall for free-slip boundary conditions and different magnitudes of the rheological parameter $\eta_c$

Although the normal forces exerted on the structure with a free-slip boundary are much greater than in the case of no-slip, the net horizontal forces $F$ that the cylinder sustains due to the action of the moving ice are smaller in the former case. This is illustrated in Table 1 in which the values of $F$ (obtained by integration of the $N_r$ and $N_{r\theta}$ components in a wind direction over the range $0 \leq \theta \leq 2\pi$) are listed for the set of the $\eta_c$ parameter values used in the simulations whose results are illustrated in the preceding plots. Hence, $F$ are the maximum values of the net horizontal loads exerted by floating ice that is 0.2 m thick and driven by wind with a speed of 30 ms$^{-1}$. For comparison, the magnitudes of $F$ calculated for a smaller cylinder, with a radius of $R_0 = 5$ m, and a larger cylinder, $R_0 = 20$ m, are also presented. We note that the value of the net force $F \approx 1.14$ MN for the $R_0 = 5$ m

cylinder, that is with a diameter of 10 m, with a free-slip wall and linearly viscous ice rheology, is about 15 per cent smaller than the respective horizontal force exerted on a rectangular structure of comparable dimensions, namely a width of 10 m, normal to the wind direction, and length of 20 m, which was investigated in Staroszczyk (2003) – see Fig. 4 in that paper.

**Table 1.** Values of the total horizontal force $F$ exerted on the structure by the ice cover as a function of the rheological parameter $\eta_c$, for different cylinder diameters $R_0$ and boundary conditions on the wall ($\eta_c \to +\infty$ corresponds to the linearly viscous solution)

| $\eta_c$ [s$^{-1}$] | $F$ [$MN$] | | | | | |
|---|---|---|---|---|---|---|
| | $R_0 = 5$ m | | $R_0 = 10$ m | | $R_0 = 20$ m | |
| | no-slip | free-slip | no-slip | free-slip | no-slip | free-slip |
| $+\infty$ | 1.142 | 0.890 | 1.342 | 1.138 | 1.513 | 1.355 |
| $1 \times 10^{-4}$ | 1.026 | 0.859 | 1.296 | 1.114 | 1.497 | 1.343 |
| $5 \times 10^{-5}$ | 0.838 | 0.780 | 1.183 | 1.050 | 1.454 | 1.309 |
| $1 \times 10^{-5}$ | 0.669 | 0.490 | 0.792 | 0.615 | 0.989 | 0.828 |

In Figures 6 and 7 we illustrate the distribution of the radial and circumferential stresses, $\sigma_{rr}$ and $\sigma_{\theta\theta}$, in the ice cover in the vicinity of the structure, for the case of a free-slip boundary. Presented are the respective values along the coordinate lines $\theta = 0$ (windward side of the cylinder) and $\theta = 180^\circ$ (leeward side) obtained for various values of the parameter $\eta_c$. The plots in both figures show that the extent of the region behind the cylinder ($\theta = 180^\circ$) in which the stresses are significantly reduced due to the divergence of ice is limited to the distance of several radii of the cylinder. In front of the structure ($\theta = 0$) the stresses $\sigma_{rr}$ and $\sigma_{r\theta}$ are very little affected by the rheological response of the ice, as is the case for the forces $N_r$ and $N_{r\theta}$ on the cylinder wall, previously demonstrated in Figs. 3 to 5.

Finally, we investigate the bending of the floating plate described by equation (27). This mode of deformation is due to the mechanism of creep buckling of the plate which leads, after a sufficiently long time, to the plate breaking once the tensile stresses in ice exceed its flexural strength. For the sake of simplicity of the analysis, we confine attention to the small domain of the ice cover in the immediate vicinity of the cylinder on its windward side, a place where the in-plane compressive stresses reach the greatest magnitudes and, therefore, the buckles grow at the fastest rate. Accordingly, we analyse the transverse deformation of ice along the coordinate line $\theta = 0$, that is, along the direction of wind. We define this direction by the axis $x$, with its origin on the structure wall, so that $x = r - R_0$ on the radius $\theta = 0$. In a matrix form, (27) can be expressed by

$$\boldsymbol{C}\dot{\boldsymbol{w}} + \boldsymbol{K}\boldsymbol{w} = 0, \tag{34}$$

where the vector $\boldsymbol{w}$ includes the values of the plate displacements at nodal points. We note that the elements of both matrices $\boldsymbol{K}$ and $\boldsymbol{C}$ depend on the horizontal ice velocities (the latter determining, through the invariant $\eta$, the ice viscosities). The

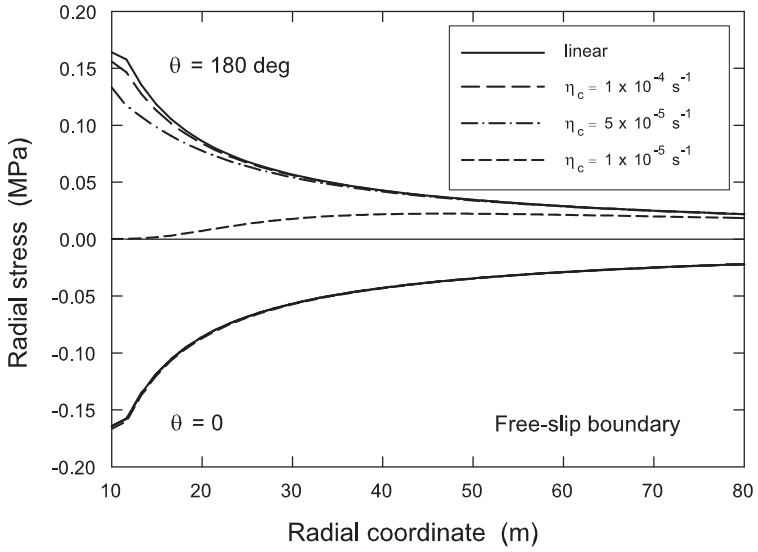


**Fig. 6.** Variation of the radial stresses $\sigma_{rr}$ with the distance $r$ along the coordinate lines $\theta = 0$ and $\theta = 180^\circ$ for free-slip boundary conditions and different values of the rheological parameter $\eta_c$

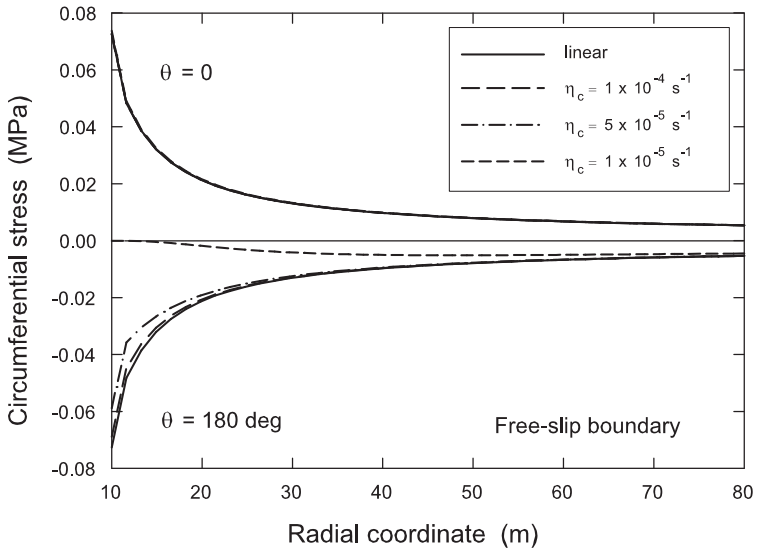


**Fig. 7.** Variation of the circumferential stresses $\sigma_{\theta\theta}$ with the distance $r$ along the coordinate lines $\theta = 0$ and $\theta = 180^\circ$ for free-slip boundary conditions and different values of the rheological parameter $\eta_c$

time-integration of the above system of equations is carried out by the standard $\Theta$-method. Application of this method to (34) yields the relation which connects the solution vectors $\boldsymbol{w}_n$ and $\boldsymbol{w}_{n+1}$ at two consecutive time instants $t_n$ and $t_{n+1}$ by

$$[\boldsymbol{C} + \Theta \Delta t \boldsymbol{K}]\, \boldsymbol{w}_{n+1} = [\boldsymbol{C} - (1 - \Theta)\Delta t \boldsymbol{K}]\, \boldsymbol{w}_n, \quad n = 0, 1, 2, \ldots, \tag{35}$$

where $\Delta t = t_{n+1} - t_n$ is the time step length. Unconditional stability of the integration scheme requires $\Theta > 0.5$; we have adopted the value of $\Theta = 0.6$ in calculations. In order to determine the bending and twisting moments (24) one also needs the time-rate of the deflection vector, $\dot{\boldsymbol{w}}$. The latter is calculated directly from (34), given a current vector $\boldsymbol{w}_n$. The system of first-order differential equations (34) requires plate deflection $w$ to be prescribed at the start of deformation. Following Sanderson (1988) and Staroszczyk and Hedzielski (2004), we assume the initial ice plate deflection $w$ to consist of small perturbations about the surface $w = 0$. For simplicity, we assume that these initial perturbations vary along the $x$ axis, but do not change in the lateral direction. Hence, we express $w$ at $t = 0$ as the sum of thirty harmonic in $x$ components, given by

$$w_0(x) = \sum_{i=1}^{30} \pm w_0^{(i)} \sin(i\pi x/L), \tag{36}$$

where the signs ($\pm$) are chosen at random, and all the component amplitudes $w_0^{(i)}$ are assumed to be equal and such that the maximum initial displacement $w_0 = 0.001$ m. $L$ denotes the longest half-wavelength of the initial perturbation, chosen here to be 20 m so that the shortest initial perturbation length is $L/30 \approx 0.67$ m. The critical tensile stress in ice at which the plate is considered to start to fail due to the development and subsequent opening of cracks, is calculated by assuming that the ice fracture toughness is 0.1 MPa $\mathrm{m}^{1/2}$ (Sanderson 1988). It has been assumed that ice fails when the length of vertically aligned cracks is equal to $h/10$.

Figure 8 $w(x, t)$ of the plate of thickness $h = 0.2$ m, pressed against the cylinder with a radius of $R_0 = 10$ m by a wind blowing with a velocity of 30 $\mathrm{ms}^{-1}$; with the ice rheological parameter $\eta_c = 1 \times 10^{-5}$ $\mathrm{s}^{-1}$ and ice field size $R_{\max} = 500$ m. The plots illustrate how the plate displacements, displayed at time intervals $t = 80$ s, gradually change from the initial random distribution of small-amplitude perturbations apparent in Figure 8a for smaller values of $t$, into the increasingly regular pattern shown in Figure 8b for larger values of $t$. We observe that in time, the creep bending deformation of the plate becomes dominated by a single buckling mode of the half-wavelength $L_0 \approx 3.7$ m, while the other, shorter and longer modes present in the initial composition of $w_0(x)$ disappear, since they grow (and the longest modes even decay) at smaller rates than the dominant component of length $L_0$. The curve for $t = 740$ s shows the plate deflection at the onset of its flexural failure due to maximum tensile stress in ice exceeding its strength. We

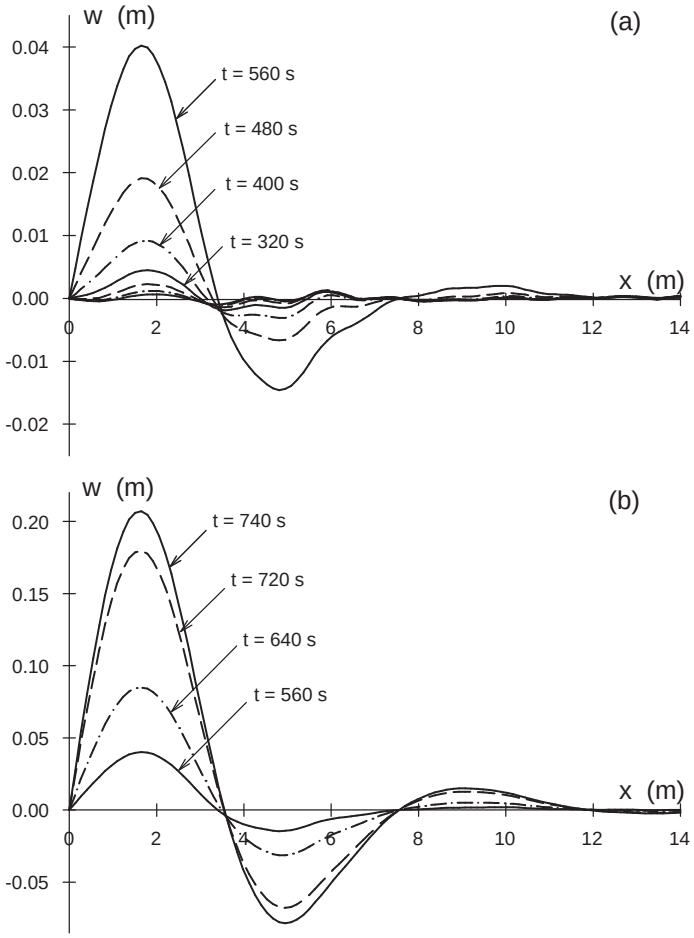


**Fig. 8.** Evolution of the deflection $w(x,t)$ of the plate of thickness $h = 0.2$ m in the vicinity of the cylinder: (a) for $t \leq 560$ s, (b) for $t \geq 560$ s

note that the maximum plate deflection at the failure time is roughly equal to the thickness of the ice. After the critical time $t_c = 740$ s the plate breaks up, starting a series of ice–structure interaction events irregular in time, with strongly varying magnitudes of the contact forces between the ice and the cylinder.

## 5. Conclusions

The forces which a floating ice field, driven by wind drag stresses, exerts on a rigid cylinder have been determined by assuming that the creep behaviour of ice is viscous. The specific form of the constitutive law (based on the Reiner-Rivlin equation) that is investigated in this work, describes the ice response in terms of

two viscosities. The latter are assumed to be constant in converging ice flow, and strongly non-linear in a narrow range of positive dilatation rates at the start of diverging flow, in order to incorporate the observed phenomenon of a rapid weakening of floating ice in tensile deformations. The variation of the ice viscosities during the transition between the converging and diverging flows has been assumed to be smooth rather than abrupt (such as that described by the Heaviside step function), since the discontinuities in the ice response give rise to numerical instabilities, as was demonstrated in earlier studies. The results of numerical calculations conducted for different ice rheological parameters and boundary conditions at the ice – structure interface have shown, for the rheological parameters explored, that the decrease in the ice strength in diverging regions reduces the forces sustained by the cylinder by about 40 per cent for a no-slip interface, and about 45 per cent for a free-slip interface, both compared with the corresponding values predicted by the linearly viscous flow law. The comparison of the net horizontal forces calculated for the two types of boundary conditions shows that the loads exerted on the cylinder in the case of the (probably more realistic) free-slip conditions are about 20 to 25 per cent less than in the case of a no-slip boundary. However, it has turned out that, despite the smooth variation of the ice viscosities at the near-zero positive dilatation rates, it is difficult to maintain the stability of the numerical scheme in the case of viscosity magnitudes reduced by more than $10^3$ to $10^4$ times compared to the respective values for converging deformations. Therefore, in the calculations the viscosities in diverging regions have been reduced by a factor of no more than $10^3$ compared to the linear case. It seems that the numerical difficulties mentioned above are caused by the occurrence in our problem of extended free boundaries between the ice and open water, since such difficulties were not encountered in previous analyses (Schulkes, Morland and Staroszczyk 1998, Morland and Staroszczyk 1998) in which most of the boundaries were fixed and rigid. In fact, even in the problem investigated in this work, no numerical problems arise when the ice velocities, instead of zero stresses, are prescribed at the outer edge of the ice field.

## References


Gray J. M. N. T., Morland L. W. (1994), A Two-Dimensional Model for the Dynamics of Sea Ice, *Phil. Trans. R. Soc. Lond.*, A 347, 219–290.

Hibler W. D. (1979), A Dynamic Thermodynamic Sea Ice Model, *J. Phys. Oceanogr.*, **9**, 815–845.

Hibler W. D., Ip C. F. (1995), The Effect of Sea Ice Rheology on Arctic Buoy Drift, *ASME AMD*, **207**, 255–263.

Morland L. W., Staroszczyk R. (1998), A Material Coordinate Treatment of the Sea-Ice Dynamics Equations, *Proc. R. Soc. Lond.*, A **454** (1979), 2819–2857.

Overland J. E., Pease C. H. (1988), Modeling Ice Dynamics of Coastal Seas, *J. Geophys. Res.*, **93** (C12), 15619–15637.

Sanderson T. J. O. (1988), *Ice Mechanics, Risks to Offshore Structures*, Graham and Trotman, London.

Schulkes R. M. S. M., Morland L. W., Staroszczyk R. (1998), A Finite-Element Treatment of Sea Ice Dynamics for Different Ice Rheologies, *Int. J. Numer. Anal. Meth. Geomech.*, **22** (3), 153–174.

Sjölind S. G. (1985), Viscoelastic Buckling Analysis of Floating Ice Sheets, *Cold Reg. Sci. Technol.*, **11** (3), 241–246.

Smith R. B. (1983) A Note on the Constitutive Law for Sea Ice, *J. Glaciol.*, **29** (101), 191–195.

Staroszczyk R. (2003), Finite Element Simulations of Floating Ice – Engineering Structure Interactions, *Arch. Hydro-Eng. Environ. Mech.*, **50** (3), 251–268.

Staroszczyk R., Hedzielski B. (2004), Creep Buckling of a Wedge-Shaped Floating Ice Plate, *Eng. Trans.*, **52** (1–2), 111–130.

Timoshenko S., Woinowsky-Krieger S. (1959), *Theory of Plates and Shells*, McGraw-Hill, New York, 2nd edn.

Wang Y. S., Ralston T. D. (1983), Elastic-Plastic Stress and Strain Distributions in an Ice Sheet Moving against a Circular Structure, *Proc. Seventh International Conf. on Port and Ocean Engineering under Arctic Conditions,* Helsinki 1983, 940–951.